



ALGORITHMS FOR THE EXTRACTION OF VARIOUS DIAMETER VESSELS

B. TREMBLAIS, A. S. CAPELLE-LAIZE AND B. AUGEREAU

Laboratory SIC – EA 4103 University of Poitiers
Bd Marie et Pierre Curie – Bat SP2MI
86962 Futuroscope-Chasseneuil, France
Fax: 33(0)5 49 49 65 70
Email: tremblais@sic.sp2mi.univ-poitiers.fr

Received November 21st, 2005; Accepted February 28th, 2006; Published April 27th, 2007

Abstract - In this communication we propose a new and automatic strategy for the multi-scale extraction of vessels. The objective is to obtain a good representation of the vessels. That is to say a precise characterization of their centerlines and diameters. The adopted solution requires the generation of an image scale-space in which the various levels of details allow to process arteries of any diameter. The proposed method is implemented using the Partial Differential Equations (PDE) and differential geometry formalisms. The differential geometry allows, by the computation of a new valley response, to characterize the centerlines of vessels as well as the bottom lines of the valleys of the image surface. The information given by the centerlines and valley response at different scales are used to obtain the 2D multi-scale centerlines of the arteries. To that purpose, we construct a multi-scale adjacency graph which permits to keep the K strongest detections. Then, the detection we obtain is coded as an attributed graph. The suggested algorithm is applied in the scope of two kinds of angiograms: coronaries and retinal angiograms

Keywords: Medical Imaging, multi-scale analysis, PDE, valley, X-ray angiograms, vessels.

INTRODUCTION

The work presented in this paper is a part of broader project, which consists in developing a general method to detect, rebuild, analyze and visualize coronary arteries. The development of a three-dimensional (3D) synthesized image will allow to carry out blood flows simulations on pathological arterial segments. Consequently, it will bring out a symptomatic indication and a better hemodynamic evaluation of the repercussion of a stenosis on the myocardic perfusion. The medical practitioner will therefore be able to decide on a treatment that suits the pathology. Currently, the 2D X-ray angiography is the most widely spread, and one of the best vessels-adapted imagery systems for studying coronary arteries. It is able to reveal projections of the arteries along several incidences. When there is only a low number of incidences, the use of a three-dimensional geometrical model of the vessels is necessary to mitigate the scarce information provided by the projection. In this context, the vessels are often modeled by generalized cylinders. Hence, they are characterized by a set of cross sections centered on a virtual trajectory going through the center of the vessels. According to [1], the general process of a 3D reconstruction includes the following

steps: 1) angiogram preprocessing: this step consists in enhancing the vessels in regard to the background of the image; 2) skeletonization and edges extraction: this step consists in detecting the points belonging to the virtual path going through the vessels and detecting those belonging to the boundary of the vessels; 3) 2D features formation: the detected points must be organized in order to form the two structural entities: the skeleton and the edges of the arteries. The first one gives the localization and the topology of the arterial tree, and the second one gives the morphology of the detected vessels; 4) matching of the 2D detected features: here, the point is to match the detected arterial segments to the corresponding anatomical structures; 5) 3D reconstruction: the skeleton detection from each incidence allows to estimate the three-dimensional localization of the vessels skeleton. The edges detection provides an estimation of the generalized cylinders cross sections parameters.

In the present work, we focus on the three preliminary steps of the 3D-reconstruction, by proposing a new algorithm for the multi-scale analysis of the vessels. It is based on Partial Differential Equations (PDE) and differential geometry frameworks.

This paper is organized as following: Section 2 presents previous works on vessels detection; in Section 3, after some reminders of differential geometry, we propose a new valley response; in Section 4, we describe a multi-scale vessels detection algorithm; in Section 5, we present several experimental results. Finally we draw the main conclusion in Section 6.

PREVIOUS WORKS

To process 2D X-ray angiograms, several constraints and difficulties must be taken into account: the luminance of these images depends greatly on the capturing conditions (x-ray intensity, angle of incidence, x-ray absorption of the organs...); the ribs, the vertebrae and the catheter, which have no interest for a coronographic examination, but look like blood vessels and can therefore disturb the automatic detection processes; the non-uniform diffusion of the contrast agent; the variability of the arteries size; the X-ray system noise. All of these constraints led to develop specialized detection or segmentation techniques. One can distinguish five main categories of techniques:

1) *Mathematical morphology techniques*: Toumoulin *et al.* [2] use a combination of closing and opening mathematical morphology operators to enhance the vessels of subtracted angiograms. They use a modified grey-level skeleton algorithm and a top-hat operator to extract local maxima. A binary skeleton is extracted. Finally they use successive dilations and comparisons with the local gradient magnitude to detect the edges. Eiho *et al.* [3] use a top-hat operator with a structuring element whose size is related to the size of largest vessels, an erosion operator to enlarge the vessels and to reduce the noise. The resulting image is thresholded and skeletonized by thinning operations. Finally the authors use a watershed transform based on the centerline and background markers.

2) *Tracking techniques*: these techniques require user interactions to define beginning, ending or in-between points or cross-sections [4,5]. A least cost algorithm is then ran to connect the manually selected points. The cost function is generally based on greylevels [5,6,7] and edge information like the gradient norm, Laplacian zeros, parallelism response... [8,9]. The least cost algorithms are related to the research of the least cost path in a valued

graph. Suggested solutions are based on the A* algorithm [4,5,9], on recursive sequential tracking [8,7,10], or front propagation [11,12].

3) *Deformable models techniques*: these techniques consist in a manual initialization of an opened skeleton or edge, generally modeled by a spline, which is iteratively deformed in such way that the points belonging to the spline minimize a global deformation energy function. This energy function is divided between an internal deformation term, controlling the “tension” and the “rigidity” of the spline, and an external deformation term which defines the attraction of the spline on the skeleton or on the edge. The choice of this external energy usually depends on the applications and the authors. For example Klein *et al.* [13] use “stretched-Gabor” filters [14], whereas Chen *et al.* [15] prefer using the local minima of the image intensity.

4) *Multi-resolution techniques*: these techniques give images at several resolutions allowing to simplify or accelerate some “conventional” image processing tasks. Different approaches, like wavelets [16,17] or Gaussian pyramids [18] are used to provide the different resolutions. The main drawback of these techniques is the difficulty to follow the structures across different image resolutions. Some applications of these techniques to vessels detection have been suggested by [19], [20] and [21].

5) *Multi-scales techniques*: these approaches consist in computing a response of the sought structure at different chosen scales. The scale giving the highest response is related to the size of this structure. A multi-scale analysis is generally composed of two main steps: a feature extraction step where the skeleton or edges are extracted at different scales and a scale-space fusion step where the meaningful information of the scale-space is summarized from all of the scales in one image to simplify the decision step (Fig. 1). Numerous works for vessels detection use these techniques [22,23,24,25,26,27,28,29].

Among all these techniques, most of them first extract the edges and then define the skeleton as the centerline of the detected edges while others prefer to detect the skeleton first and then the edges. We consider that this latter solution is the most adapted to our application. In fact, near stenosis area, edge points on both sides of the vessels may not always be detected simultaneously. Besides, it has been shown that the center points localization depends on the

edge operator. Here, we aim at detecting the whole arterial tree, first of all to simplify the matching step, but also to limit as much as possible the surgeon's work. Contrary to most of the literature techniques, we propose an automatic detection where the surgeon can quickly select good and bad detections. This way, no fastidious and time expensive initialization step is needed.

Here we chose to use a multi-scale approach for the following issues: 1) it allows an automatic and global detection of vessels of various diameters; 2) it does not require initialization steps; 3) it provides a family of same sized images which simplify the fusion process.

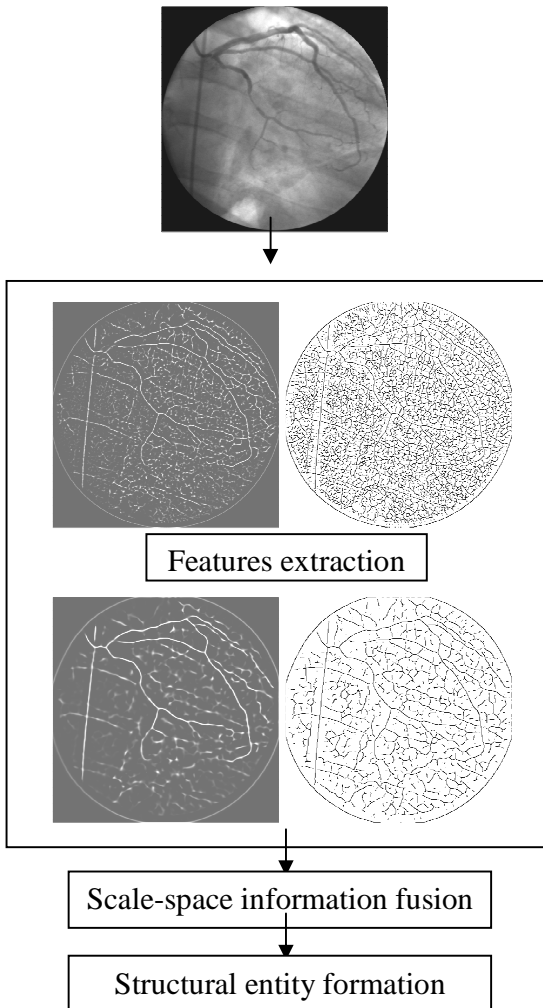


Figure 1. The general scheme of a multi-scale analysis detection.

FEATURES EXTRACTION

Characterizing vessels by a response function

Coronary arteries obtained by X-ray angiography are elongated and dark structures on the image background. Arteries tubular nature implies a greater absorption of X-ray in the axial part of the arteries than on their wall. Therefore, if we study the intensity along a profile perpendicular to the local direction of an artery, the skeleton appears to be located in the same place that the local minima of the intensity function (Fig. 2). Besides, if we consider the image as a surface of R^3 , then the coronary arteries become valleys within the relief of the image surface. So, to extract the skeleton means to locate the points in the bottom of these valleys. Besides, as shown by Chen and al. [30], even if bottom points do not generally correspond to centerlines points, their detection is highly stable. Throughout this article, we use the following notations and terminology to design points or sets of points of the relief map. A valley is an elongated depression between mounts. The set of points located in the bottom of a valley is called a bottom-line. Differential geometry allows to generalize the research of local extrema on one-dimensional real functions to multidimensional functions. This is the reason for using this mathematical framework in this article.

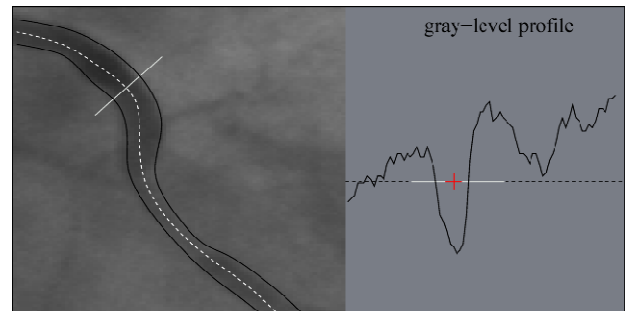


Figure 2. The profile of intensity following a perpendicular direction to the vessel.

We consider the image I as the map $I : \Omega \subset R^2 \rightarrow R$. The first and second local partial derivatives of the image are defined by $I_x, I_y, I_{xx}, I_{yy}, I_{xy}$.

$\nabla = \left(\frac{\partial}{\partial x}, \frac{\partial}{\partial y} \right)^t$ denotes the gradient operator. Given a vector in R^2 , we denote the first derivative along a , $I_a = \nabla I \cdot a$. Given Σ a two-dimensional manifold

locally embedded in R^3 , the image is then modeled by a map $S : \Sigma \rightarrow R^3$.

$$S = (\sigma^1, \sigma^2) = (X^1(\sigma^1, \sigma^2), X^2(\sigma^1, \sigma^2), X^3(\sigma^1, \sigma^2)), \quad (1)$$

σ^1 and σ^2 being the curvilinear coordinates of the image surface. For each point of S the tangent space T

is the plane created by the vectors $S_{\sigma^1} = \frac{\partial S(\sigma^1, \sigma^2)}{\partial \sigma^1}$ and

$S_{\sigma^2} = \frac{\partial S(\sigma^1, \sigma^2)}{\partial \sigma^2}$. The first fundamental form allows to

define a metric g_Σ on Σ . It can be written as a positive definite symmetric form:

$$d_s^2 = \sum_{i,j=1}^2 d_{ij} g_{\sigma^1}^i g_{\sigma^2}^j \quad (2)$$

which associated matrix is:

$$F_I = \begin{pmatrix} g_{11} & g_{12} \\ g_{21} & g_{22} \end{pmatrix} \quad (3)$$

The second fundamental form represents the curvature of curves drawn on the surface. It is defined by the matrix:

$$F_2 = \begin{pmatrix} \langle \bar{n}, S_{uu} \rangle & \langle \bar{n}, S_{uv} \rangle \\ \langle \bar{n}, S_{uv} \rangle & \langle \bar{n}, S_{vv} \rangle \end{pmatrix} \quad (4)$$

where $\langle \dots, \rangle$ is the inner-product defined on R^3 and \bar{n} is the normal vector to the surface such that $(S_{\sigma^1}, S_{\sigma^2}, \bar{n})$ is a direct basis. The principal curvatures, $k_i, i \in \{1, 2\}$, and the principal directions of the extrema of the image's surface, $v_i, i \in \{1, 2\}$, are respectively the eigenvalues and eigenvectors of $A = F_1^{-1} F_2$.

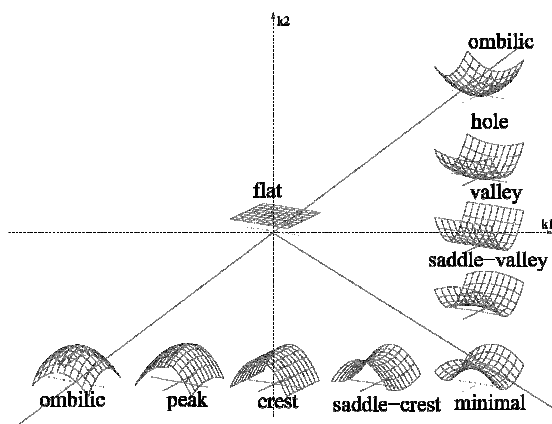


Figure 3: The classification of the image's surface points in regard with k_1 and k_2 .

We present in Table 1 the calculation of the fundamental forms, according to two conventional choices of g_Σ for $S(x, y) = (X^1(\sigma_1, \sigma_2) = x, X^2(\sigma_1, \sigma_2) = y, X^3(\sigma_1, \sigma_2) = I(x, y))$. \mathcal{W} and \mathcal{H} are respectively called the Weingarten and Hessian matrices. We notice that both metrics are invariant to translations and rotations in the spatial variables transformations, but the metric induced by R^3 is the only one giving the invariance with regard to the spatial unit transforms.

The great interest with the principal curvatures is that they allow to classify the points of the surface according to the following categories: valley, crest, flat, pit, peak, saddle and minimal (see Fig. 3). Consequently, a point of the valley is mathematically a point of the image's surface such that $k_1 > 0$ and $k_2 = 0$.

In practice, the luminance variations and the noise in real images make the detection of pure valleys almost impossible ($k_1 > 0$ and $k_2 = 0$). In regard with the previous definitions, the search domain of valley points V is such that $k_1 > 0$ (Fig. 3). That is to say the points that verify:

$$\begin{cases} k_1 \neq k_2 \\ k_1 \neq -k_2 \\ \max(|k_1|, |k_2|) = k_1 \end{cases}$$

Table 1. Differential characteristics in regard with the choice of the metric \square .

Metric	Euclidian	Induced
F_1	$\begin{pmatrix} 1 & 0 \\ 0 & 1 \end{pmatrix}$	$\begin{pmatrix} 1+I_x^2 & I_x I_y \\ I_x I_y & 1+I_y^2 \end{pmatrix}$
F_2	$\mathcal{H} = \begin{pmatrix} I_{xx} & I_x I_y \\ I_x I_y & I_{yy} \end{pmatrix}$	$\frac{1}{\sqrt{1+I_x^2+I_y^2}} \mathcal{H}$
A	\mathcal{H}	$\mathcal{W} = F_1^{-1} F_2$

In other words we have extended the search domain to saddle-valley and hole points excluding

ombilic and minimal points. Among the points of \mathbf{V} , we need now to extract the points belonging to the bottom-lines. For each point, we can define a bottom-line membership degree function \mathbf{D} depending on the principal curvatures. In the following, we will call \mathbf{D} a valley response. A few functions have already been suggested in the literature, such as $\mathbf{D}_1(k_1, k_2) = \sqrt{k_1^2 + k_2^2}$ and $\mathbf{D}_2(k_1, k_2) = (k_1^2 + k_2^2)^2$ by Lindeberg [23], and $\mathbf{D}_3(k_1, k_2) = k_1$ by Nasser [23]. It is worth noticing that the functions \mathbf{D}_1 , \mathbf{D}_2 and \mathbf{D}_3 may have very high values where the local surface does not correspond to a valley. So we suggest that the \mathbf{D} function should rather verify the following properties for the points of \mathbf{V} :

1. $\mathbf{D}(k_1, k_2) = \mathbf{D}(k_1, -k_2)$
2. $\lim_{k_1 \rightarrow 0, k_2 \rightarrow 0} \mathbf{D}(k_1, k_2) = 0$
3. $\mathbf{D}(k_1, k_2)$ increasing in k_1
4. $\mathbf{D}(k_1, k_2)$ decreasing in k_2 (both sides of the k_1 axis)

Those conditions are verified by the function $D(k_1, k_2) = |k_1 - k_2| / |k_1 + k_2|$ (see Fig. 4). According to us, a bottom-line point is then a point of \mathbf{V} which is a local maximum of the response \mathbf{D} in the direction of \mathbf{V}_1 .

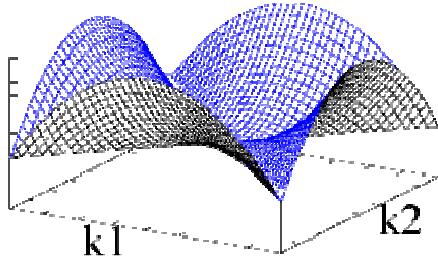


Figure 4. $D(k_1, k_2) = |k_1 - k_2| / |k_1 + k_2|$.

Definition 1. A bottom-line point verifies:

$$\begin{cases} k_1 & \neq k_2 \\ k_1 & \neq -k_2 \\ \max(|k_1|, |k_2|) & = k_1 \\ \nabla \mathbf{D} \cdot \mathbf{v}_1 & = 0 \end{cases} \quad (7)$$

Our experiments [31] show that using the eigenvalues of the Weingarten matrix for the calculus of \mathbf{D} and the eigenvectors of the Hessian matrix, which are less noise sensitive, gives better results, especially in regard with the continuity of the extraction. Fig. 5 gives an example of the vessels centerlines extraction on an angiogram. One can see that vessels are well localized. Besides, their detection is almost continuous.

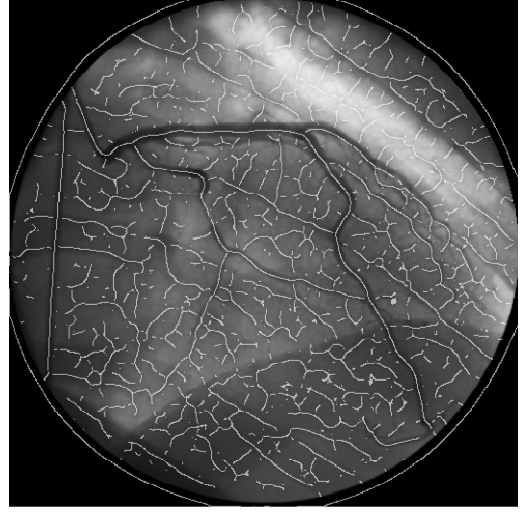


Figure 5. Superimposition of the extraction with an angiogram.

MULTI-SCALE EXTRACTION OF ELONGATED STRUCTURES

Multi-scale detection of the bottom-lines

In order to study vessels of various sizes and to regularize the calculus of the derivatives, we decide to perform a linear multi-scale analysis based on a PDE process coming from the heat equation [32,33]:

$$\begin{cases} \frac{\partial I(x, y)}{\partial t} & = \Delta I(x, y, t), \forall (x, y) \in \Omega \\ I(x, y, t) & = I_0 \\ \frac{\partial I}{\partial n} \Big|_{\partial \Omega} & = 0 \end{cases} \quad (8)$$

Where $I_0(x, y)$ is the initial image and $\partial \Omega$ is the boundary of Ω . In order to process the image at different scales and to take into account large scales, this equation is approximated by an iterative explicit discretization scheme.

Scale-space parameters setting

At this point, we now have to set the number p of scales and their distribution in the range $[\sigma_{\min}, \sigma_{\max}]$. The ideal case would be to know the various vessels sizes and then to choose the study scale according to that. But in practice, the task is more difficult because we just have an estimation of the widest arteries size. To determine the minimal scale σ_{\min} , we have taken into account the sampling problems (i.e. aliasing) by choosing $\sigma_{\min} = 1.0$. As many authors did before [24,22], we modeled the vessels by generalized cylinders with a symmetric bar-profile of width ω , in

order to estimate the optimal detection scale. After some calculus, we deduce the optimal scale expression: $s_{opt}(\omega) = \omega(2\sqrt{3})^{-1}$. The maximal scale σ_{max} is empirically set according to the size of the widest arteries, that is to say about twenty pixels of width in the studied angiograms. So $\sigma_{max} = S_{opt}(20) = 5.77$.

In the scope of our application, we aim to follow the detected bottom-lines across the scale-space. A logarithmic sampling seems to be more coherent with the evolution of the image changes across the iterative process. However, to achieve this, we must take care of avoiding too high sampling steps. Experiments have indicated that for the small scales a logarithmic sampling fails with these requirements. Therefore, we suggest to use an uniform sampling towards a particular scale σ_c , and then to use a logarithmic sampling for superior scales. This almost logarithmic sampling allows to better follow the detected bottom-lines across the scale-space. We present in Table 2 the sampling sequence used for the linear multi-scale analysis of the coronary arteries.

Table 2. Scales chosen for the multi-scale analysis of the coronary arteries

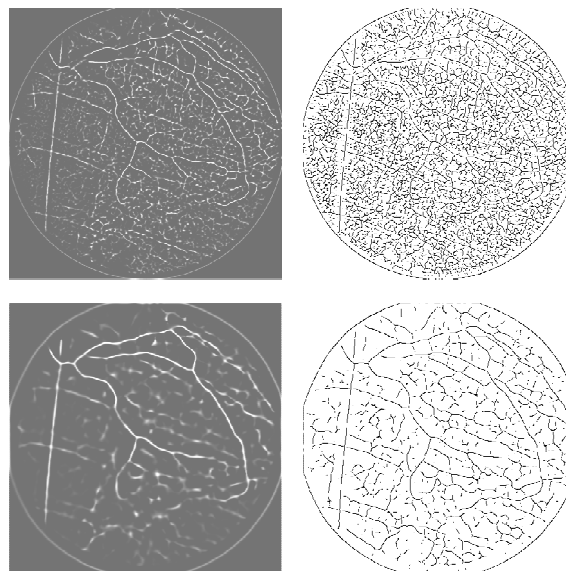
t	0.50	0.75	1.00	1.25	1.50	1.75	2.00	2.25	2.50
σ	1.00	1.22	1.41	1.58	1.73	1.87	2.00	2.12	2.23
t	2.75	3.50	4.50	5.75	7.50	9.25	12.25	15.75	-
σ	2.34	2.64	3.00	3.39	3.87	4.30	4.95	5.61	-

The multi-scale detection algorithm

Now, we present a new multi-scale algorithm for the detection of the vessels. Let $\Sigma = \{\sigma_{i \in \{1, \dots, p\}}\}$ be a set of p scales. Let $\{V_{\sigma_i}^r\}_{i \in \{1, \dots, p\}}$ and $\{BL_{\sigma_i}\}_{i \in \{1, \dots, p\}}$ respectively be the set of the valley response and the bottom-lines detection at scale σ_i which we will call the valley scale-space and the bottom-lines scale-space. Notice that the dimension of these spaces is $N+1$. Fig. 7 gives some scales of these scale-spaces for a left coronary artery. One can see the progressive disappearance of the small vessels when the scale is growing.

As Monga *et al.* did in [34], we construct a multi-scale adjacency graph from those two scale-spaces. The nodes of the graph are the points P detected at least once across the bottom-lines scale-space. That is

to say, the points for which a σ_i exists such that $BL_{\sigma_i}(P) = 1$. Each node contains all the scales σ_i verifying $BL_{\sigma_i}(P) = 1$, as well as the valley response and the directions of the principal curvatures. An edge connects two nodes if the points are adjacent or neighbors in the bottom-lines scale-space. Let $NE(P^{i-1})$, $NE(P^i)$ and $NE(P^{i+1})$ respectively be the set of the neighbors of P in the bottom-lines map at scale σ_{i-1} , σ_i and σ_{i+1} . We define the set of neighbors of P_i in the bottom-lines scale-space as the set $N(P^i) = \{NE(P^{i-1}) \cup P^{i-1}, NE(P^i), NE(P^{i+1}) \cup P^{i+1}\}$. Thus, in the two-dimensional case, nodes have 26 neighbors. By studying the bottom-lines scale-space [31], we can notice that the used detector relatively preserves the localization of the detection across the scales (the offsets do not exceed one or two pixels). Consequently, the stability hypothesis first planed by Witkin [33], “the structures which survive over a broad of scales tends to leap out the eye...”, is suitable to our purpose. According to this property we decide to prune the graph, keeping the nodes which have been detected at least N times. A lot of insignificant bottom-lines are eliminated this way. The experience shows that the value of N directly depends on the kind of image to process. In other words, this parameter can be fixed for a particular application.



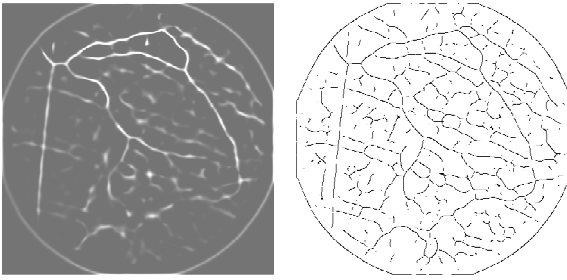


Figure 6. Left: some scales of the normalized valley scale-space, Right: some scales of the bottom-lines scale-space.

Let $\#C$ be the number of connected components of the graph, we denote by $\{CC_k\}$, $k \in \{1, \dots, \#C\}$ the set of these connected components. To each connected component we attribute the following response:

$$M(CC_k) = \frac{\sum_{P \in CC_k} R(P)}{\#CC_k} \quad (9)$$

where $\#CC_k$ and $R(P)$ respectively denote the number of nodes belonging to the connected components CC_k and the valley response corresponding to the P point, $M(CC_k)$ being the mean of the responses corresponding to the connected component CC_k . Thereafter, we also sort the connected components by decreasing order according to the $M(CC_k)$ values. By tuning the number K between 1 and $\#C$, we can keep the K "strongest" connected components. The choice of K can be leaved to the user's appreciation. Fig. 8 shows the impact of the choice of K on the multi-scale detection results. Projecting these components onto the image plane, we obtain the "shadow" of the K strongest connected components. In fact, this step allows to get a better connected arterial tree.

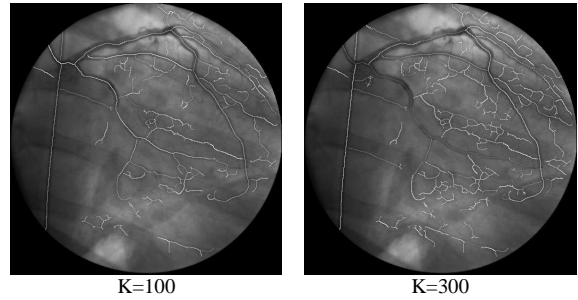
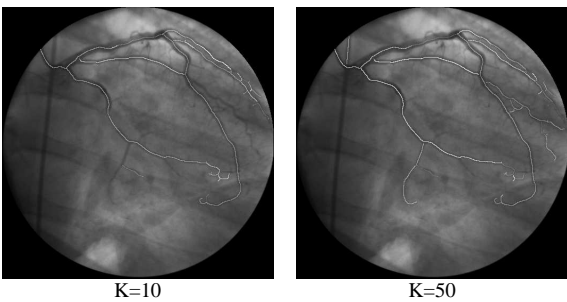


Figure 7. Some bottom-lines extractions for different values of K .

Then, a homotopic thinning algorithm [36] allows to transform the bottom-lines into one pixel width 8-connected paths. Finally, the remaining detection artifacts are eliminated by deleting low length edges. Fig. 9 shows a more synthetic description of our algorithm. It is worth noticing that this algorithm is very easy to implement comparing with a marching-line algorithm [35,37].

Structural entities formation

To form the structural entities it is necessary to find a data structure that first, allows to code the vascular tree, then acts on the detection, and finally, matches detected structures. The coronarian tree can anatomically be modeled, quite obviously, by a three-dimensional binary tree. But the projection of this tree on the X-ray sensor generally rises superimpositions and junctions. The structure of the proposed detection is consequently more complex than a simple binary tree. That is why we decide to modelize the coronarian tree by an attributed graph structure. The nodes of this graph are the detected singular points: the ending, the forks, and the junction

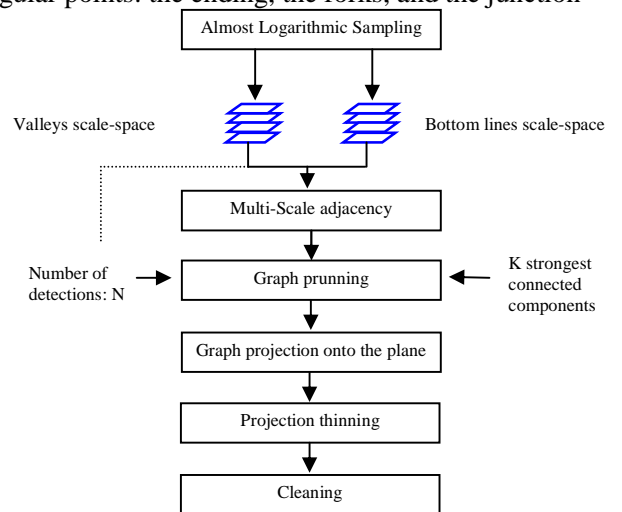
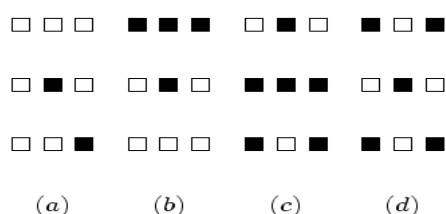


Figure 8. Fusion algorithm.

points (see Tab. 3). These singular points have been detected using the hit-or-miss operators [31]. An edge is defined by a discrete path connecting two singular points and containing the following attributes: the path points list with their own attributes (diameter, localization, principal curvatures directions...), its length and an anatomic name of the detected structure. The latter attribute allows a manual matching.

Table 3. Some local configurations of singular points. (a) end point; (b) end points; (c) bifurcation point; (d) junction point.



Diameter estimation of the vessels

Theoretically, the multi-scale analysis allows to get an estimation of the arteries' diameters by the optimal scale determination. When one samples the scale variable, it turns out that the scale giving the maximal response is rough: the scale samples are too spaced, especially with the use of a logarithmic sampling. According to this, if we denote the scale giving the maximal response σ_{\max} , we can only affirm that the optimal scale belongs to the range of scales $[\sigma_{r_{\max}-1}, \sigma_{r_{\max}+1}]$. That is why we prefer to localize the edges on both sides of the skeleton point. In order to do that, we have to analyze the profile of the image gradient in a direction perpendicular to those of the vessel. As the maximal curvatures directions are quite stable across the scale-space, we approximate it by the mean of the maximal principal curvatures directions on the whole selected scales. The gradient of the profile has been previously smoothed using a Gaussian filter to limit the noise influence. The pixels giving the maximal response to the image gradient on both sides of the skeletons will then be considered as edge points. Finally, the local diameter of the vessel is estimated by computing the Euclidean distance between these two edge points (cf. Fig. 10).

In spite of its simplicity, the suggested technique gives nevertheless a good preliminary estimation of the vessels diameters and may serve as a pathology

indicator. For further works we may imagine, as suggested by Chen *et al.* [38], an estimator based on several diameter estimation techniques.

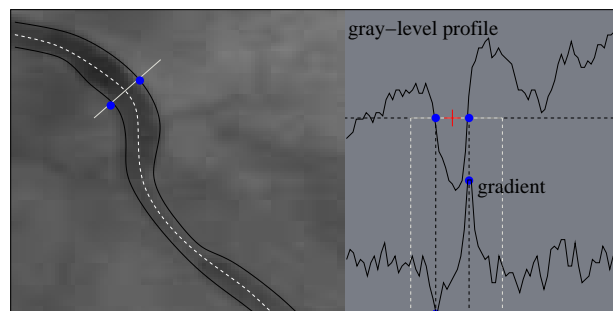


Figure 9. Diameter estimation.

EXPERIMENTAL RESULTS

X-ray coronographies

In this section, we present the results obtained using our skeleton detection algorithm applied here to two cineangiograms selected from two cineangiograms provided by the University Hospital Center of Poitiers, France. The cineangiograms have been acquired by a single plane angiographic system and digitized into 512×512 images with 8 bits of gray-level resolution. Fig. 11(a) and fig. 12(a) show two of the digitized coronary angiograms. The first one concerns a left coronary artery angiogram with RAO/CRA=12°/20°, the second one concerns a right coronary artery angiogram with LAO/CRA=89°/2°. We respectively call them “LCA-RAO12-CRA20” and “RCA-OAG89-CRA2”. The size of the widest searched artery is almost the same from one angiogram to another. So, we can use the same number of scales p for each multi-scale analysis. Furthermore, the parameter N is here fixed to 5 for this kind of images. The parameter K is individually adapted so as to favor the detection of the principal arteries, since they are the most interesting ones for the surgeon. The proposed algorithm has been implemented using the C/C++ programming language on a personal computer with CPU: AMD K7 Thunderbird 1Ghz, and 256Mo RAM running under the Linux operating system. The overall execution time for the analysis of 16 scales is usually less than 25 seconds¹.

¹It is worth noticing that the algorithm has not passed the optimization stage yet.

It is worth noticing that the skeletons are successfully and automatically extracted as one-pixel-wide near continuous 8-connected paths. That is even the case for strong stenosis like the one localized in the white circle on fig. 11(a). Besides, the result presented in fig. 12(b) shows the algorithm robustness to low contrast angiograms. One would expect such results, as throughout the whole processing sequence, we took great care about the continuity of the detection. Some arterial segments are however still disconnected when it should be the case, according to the surgeon knowledge on the real topology of the coronarian tree. In this situation there are three possibilities: 1) either the connexion might effectively exist at the “visible” intersection of the arterial segments (in this case the algorithm fails); 2) either the connexion might exist but considering the vessels overlapping its localization is uncertain; 3) either the connexion might not exist because the vessels cross each other. Conversely, two vessels could have been connected despite the fact that they should not have been. Most of the time, it happens in the case of a crossing or of an overlapping. Besides, sometimes our algorithm may detect uninteresting objects like the catheter, the patient ribs or some dark areas localized near the arteries. Under such circumstances it seems difficult to remove all these detection ambiguities having a single angiogram. We feel that at this stage it would be interesting to let the surgeon manually decide.

We show on fig. 13(b) an example of the edge detection obtained from the multi-scale skeletons detection. One can notice that edges are quite well localized and relatively continuous. This is what one would expect, since the skeletons detection was continuous itself. We notice that this method fails when the vessels are too close to one another. However, it is not really an drawback since most of the time, the surgeon chooses the projection in order to obtain an emerged sight of the studied arterial segment.

Retinal angiograms

In this application, the problems are quite similar to the analysis of coronary angiograms. The main differences principally concern the imagery system and the network vessels complexity. Fig. 14(a) shows an example of a retinal angiogram. For this image, the maximal vessel diameter is nearly inferior to twelve pixels. Resuming the previous calculus we

obtain $\sigma_{\max} = 3.46$. We choose the sampling sequence presented on Table 4.

Table 4. Scales used for the analysis of a retinal angiogram.

t	0.0	0.75	1.00	1.25	1.50	1.75	2.00
σ	1.00	1.22	1.41	1.58	1.73	1.87	2.00
t	2.25	2.50	2.75	3.50	4.50	5.75	2.25
σ	2.12	2.23	2.34	2.64	3.00	3.39	2.12

The overall execution time for a 596×603 image and 12 scales is almost less than 25 seconds. The results of the detection of retinal vessels are shown on fig. 14(b). One can notice that the quality of the results is higher than the coronary angiograms ones because we have a better contrast.

CONCLUSION

In this paper we first have introduced a valley response depending on the two principal curvatures. Doing that, we have been able to characterize points of the image surface looking like valleys as bottom-lines points. Then, we have suggested an automatic strategy for the multi-scale detection of the blood vessels going through the detection of these bottom-lines points. The proposed algorithm gives good results both in continuity terms and in localization terms, even in the case of strong stenosis and bad contrasted angiograms. Besides, the algorithm has a low computational cost, and we have shown that it is suitable to other imagery modalities. However, concerning the arteries detection, the intervention of the surgeon can still be useful to remove some ambiguities. In the future we aim at using the deformable models frameworks to reconstruct the three-dimensional representation of the interesting arterial segments.

ACKNOWLEDGEMENTS

This work was supported by the “Conseil Regional de Poitou-Charentes”, France, and the FISC consortium, France.

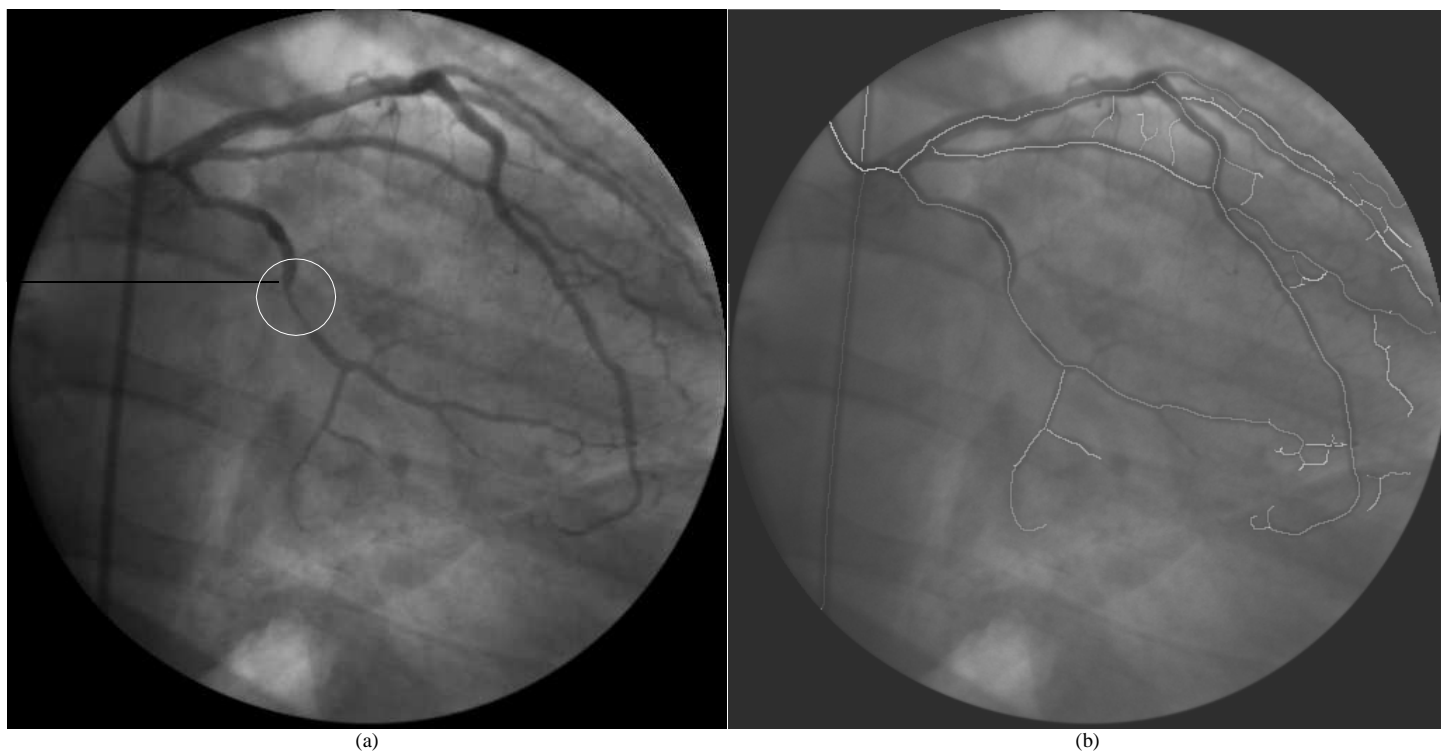


Figure 10. (a) “LCA-RAO12-CRA20” angiogram, (b) bottom-lines extraction of 11(a) with $K=100$ and $N=5$.



Figure 11. (a) “RCA-OAG89-CRA2” angiogram, (b) bottom-lines extraction of 12(a) with $K=80$ and $N=5$.

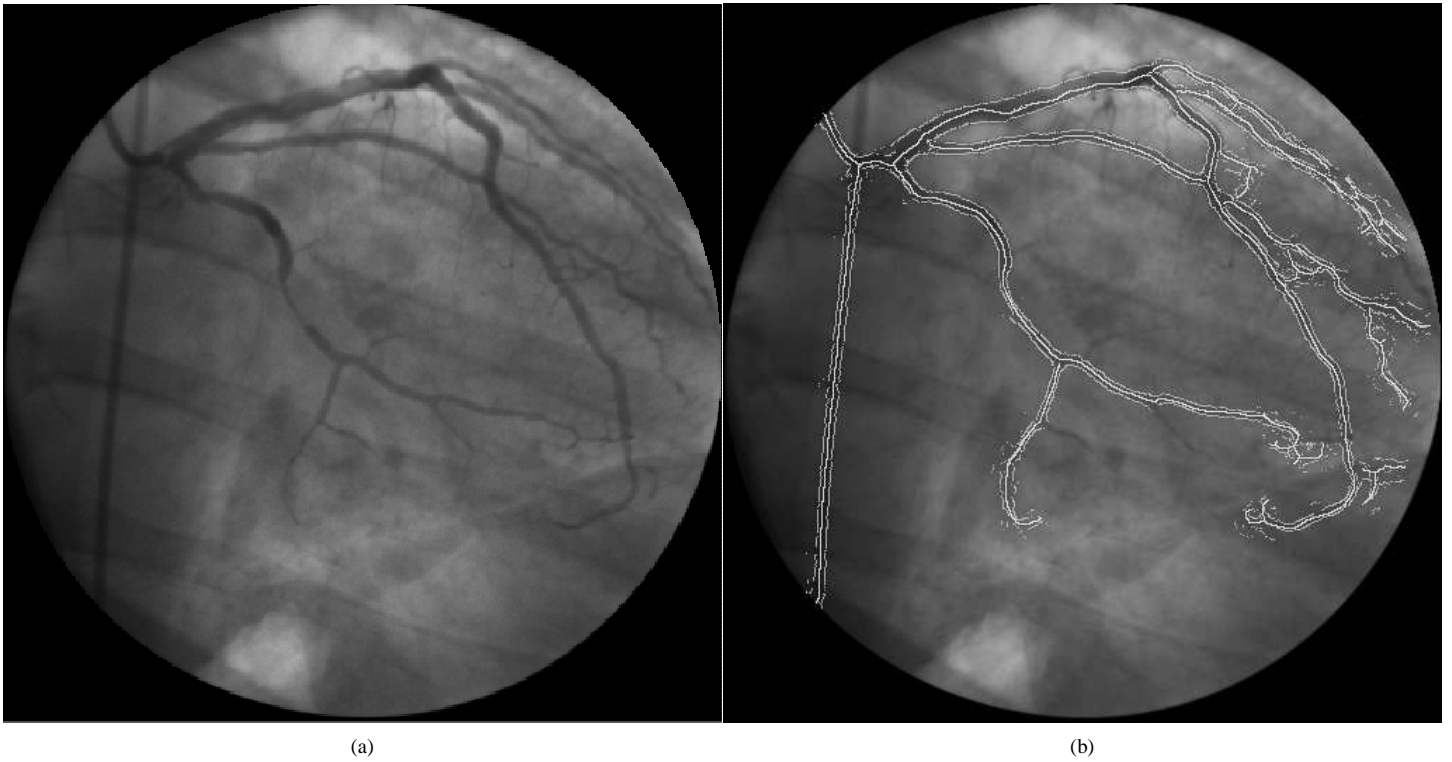


Figure 12. (a) “LCA-RAO12-CRA20” angiogram, (b) diameter estimation of “LCA-RAO12-CRA20”.

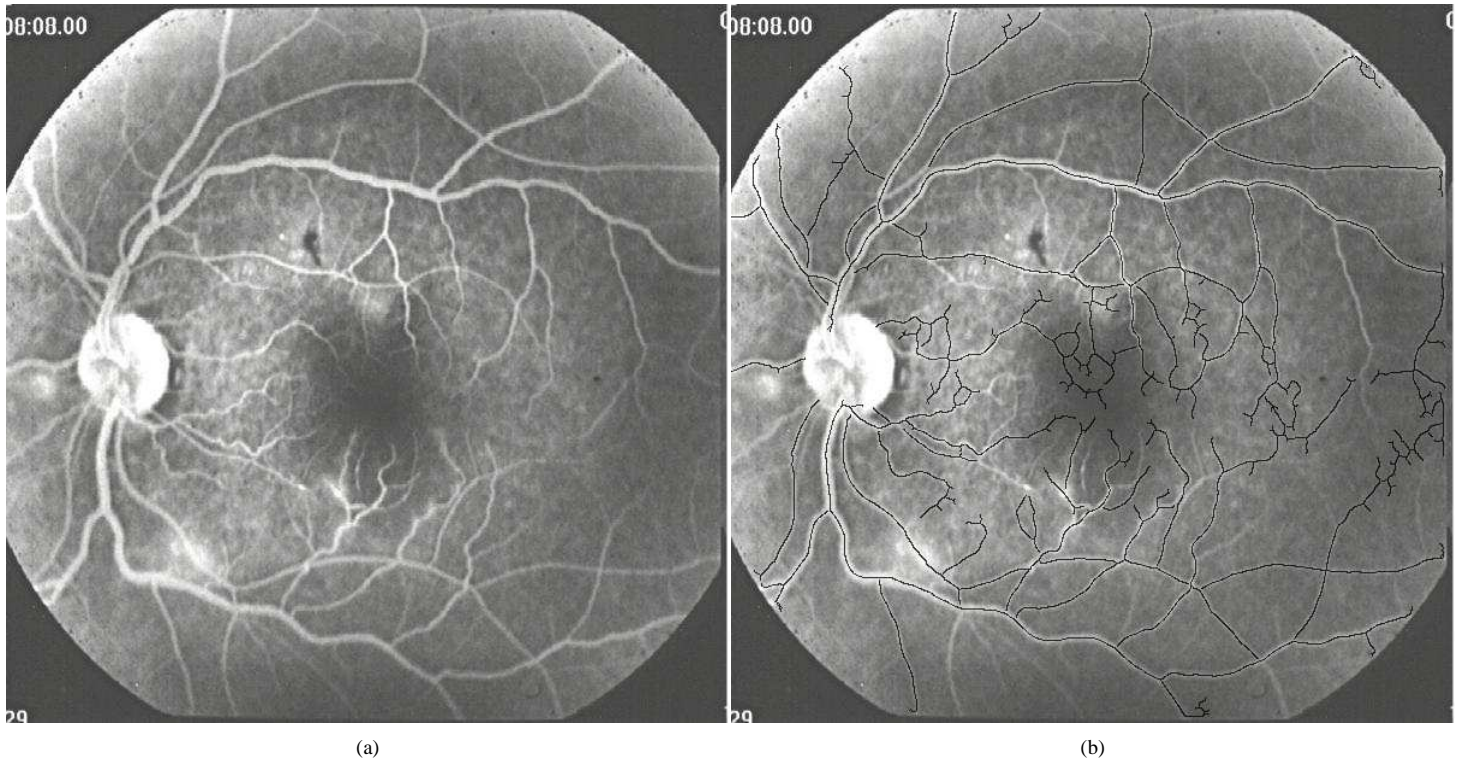


Figure 13. (a) A retinal angiogram, (b) Skeleton extraction of the vessels.

REFERENCES

1. J. Coatrieux, M. Garreau, R. Collorec, C. Roux, Computer Vision Approaches for the Three-Dimensional Reconstruction of Coronary Arteries: Review and Prospects, *Critical Reviews in Biomedical Engineering* 22 (1) (1994) 1–38.
2. C. Toumoulin, R. Collorec, J. Coatrieux, Vascular network segmentation in subtraction angiograms : a comparative study, *Medical Informatic* 15 (4) (1990) 333–341.
3. S Eiho, Y. Qian, Detection of Coronary Artery Tree Using Morphological Operator, in: *IEEE Proceedings Computer in Cardiology*, Vol. 24, Lund, Sweden, 1997.
4. M. Figueiredo, J. Leitao, A Nonsmoothing Approach to the Estimation of Vessel Contours in Angiograms, *IEEE Transactions on Medical Imaging* 14 (1) (1995) 162–172.
5. Hildebrand, S. Grosskopf, 3D Reconstruction of Coronary Arteries from X-ray Projections, in: *Proceedings of CAR'95*, 1995, pp. 201–207.
6. Pellot, A. Herment, M. Sigelle, P. Horain, Segmentation, modeling and reconstruction of arterial bifurcations in digital angiography, *Medical and Biological Engineering and Computing* 30 (1992) 576–583.
7. K. Hoffmann, A. Sen, L. Lan, C. Metz, K. chua, B. Williams, J. Esthappan, M. Fiebich, M. Mazzuco, K. Doi, Determination of 3D vessel trees from biplane images for coronary angiography, in: H. Lemke, M. Vannier, K. Inamura (Eds.), *Computer Assisted Radiology and Surgery 1997*, Elsevier Science, 1997, pp. 162–165.
8. Liu, Y. Sun, Recursive Tracking of Vascular Networks in Angiograms Based on the Detection-Deletion Scheme, *IEEE Transactions on Medical Imaging* 12 (2) (1993) 334–341.
9. L. Lecornu, J-J Jacq, C. Roux Simultaneous Tracking of the two Edges of Linear Structures, *ICIP* (1) 1994: 188–192.
10. K. Haris, S. Efstratiadis, N. Maglaveras, C. Pappas, J. Gourassas, G. Louridas, Model-Based Morphological Segmentation and Labeling of Coronary Angiograms, *IEEE Transactions on Medical Imaging* 18 (10) (1999) 1003–1015.
11. J. Jansen, G. Koning, P. de Koning, J. Tuinenburg, J. Reiber, A novel approach for the detection of pathlines in X-ray angiograms : the wavefront propagation algorithm, in: H. Lemke, M. Vannier, K. Inamura, A. Farman, K. Doi, J. Reiber (Eds.), *CARS 2002 Computer assisted Radiology and Surgery*, Springer, Paris, France, 2002, pp. 808–813.
12. F. Quek, C. Kirbas, Vessel Extraction in Medical Images by Wave-propagation and Traceback, *IEEE Transactions on Medical Imaging* 20 (2001) 117–131.
13. Klein, F. Lee, A. Amini, Quantitative Coronary Angiography with Deformable Spline Model, *IEEE Transactions on Medical Imaging* 16 (1997) 468–482.
14. F. Heitger, L. Rosenthaler, R. von der Heydt, E. Peterhans, O. Kubler, Simulation of neural contour mechanisms : From simple to end-stopped cells, *Vision Res.* 32 (5) (1992) 963–981.
15. S. Chen, J. Carroll, 3-D reconstruction of Coronary Arterial Tree to Optimize Angiographic Visualization, *IEEE Transactions on Medical Imaging* 19 (4) (2000) 318–336.
16. S. Mallat, A theory for Multi-resolution Signal Decomposition: the Wavelet transform, *IEEE Transactions on Pattern Analysis Machine Intelligence* 11 (7) (1989) 674–693.
17. Daubechies, *Ten Lectures on Wavelets*, SIAM, Philadelphia, 1992.
18. Burt, Fast filter transforms for image processing, *Computer Graphics, Image Processing*, 16 (20).
19. Basset-Merle, G. Finet, J. Lienard, and I.E. Magnin 3D reconstruction of the deformable coronary tree skeleton from two X-rays angiographic views, *Computers in Cardiology*, September 13-16, Cleveland, Ohio, USA, 1998, 757-760.
20. Munteanu, J. Cornelis, P. DeMuynck, A. Bezerianos, P. Cristea, Accurate Detection of Coronary Arteries with the Continuous Wavelet Transform, *Computers in Cardiology* 24 (1997) 601–604.
21. Z. Chen, S. Malloi, Multi-resolution Vessel Tracking in Angiographic Images Using Valley Courses, *Optical Engineering To appear*.
22. O. Monga, A. Nasser, P. Montesinos, Thin netand Crest lines : Application to Satellite Data and Medical Images, *INRIA Research Report RR-2480* (1995).
23. T. Lindeberg, Scale-space : A framework for handling image structures at multiple scales, in: *CERN School of Computing*, Egmond Zee, 1996.
24. T. Koller, G. Gerig, G. Szekely, D. Dettwiler, Multi-scale detection of curvilinear structures in 2D and 3D image data, *Fifth International Conference on Computer Vision* (1995) 864–869.
25. Y. Sato, T. Araki, M. Hanayama, H. Naito, S. Tamura, A Viewpoint Determination System for Stenosis Diagnosis and Quantification in Coronary Angiographic Image Acquisition, *IEEE Transactions on Medical Imaging* 17 (1) (1998) 121–137.
26. Lorentz, I. Carlsen, T. Buzug, C. Fassnacht, J. Weese, Multi-scale Line Segmentation with Automatic Estimation of Width, Contrast and Tangential Direction in 2D and 3D Medical Images, *CVRMed-MRCAS* (1997) 233–242.
27. Frangi, W. Niessen, K. Vincken, M. Viergever, Multi-scale vessel enhancement filtering, *MICCAI'98* 1496 (1998) 130–137.
28. Krissian, Flux-Based Anisotropic Diffusion : Application to Enhancement of 3D Angiogram *IEEE Transactions On Medical Imaging*, 22:11 (2002) 1440-1442.
29. Blondel, R. Vaillant, F. Devernay, G. Malandain, N. Ayache, Automatic trinocular 3D reconstruction of coronary artery centerlines from rotational X-ray angiography, in: *Computer Assisted Radiology and Surgery 2002 Proceedings*, Springer Publishers, Heidelberg, Paris, 2002, international Symposium on Cardiovascular Imaging - Invasive Coronary and Vascular Imaging.
30. Z. Chen, S. Malloi, Vascular tree object segmentation by deskeletonization of valley courses, *Computerized Medical Imaging and Graphics* 26 (2002) 419–428.
31. Tremblais, B. Augereau A Fast multi-scale edges detection algorithm, *Pattern Recognition Letters*, Volume 25, Number 6, (2004), 603-618.
32. Koenderink, The structure of images, *Biological Cybernetics* 50 (5) (1984) 363–370.
33. P. Witkin, Scale-space filtering, in: *AJCAI*, Karlsruhe, 1983.
34. O. Monga, R. Lengagne, R. Deriche, A multi-scale approach, *Tech. Rep. 2338*, INRIA (juillet 1994).
35. T. Lindeberg, Scale-space theory: A basic tool for analysing structures at different scales, *Journal of Applied Statistics* 21 (2) (1994) 225–270.
36. Lantuéjoul, Skeletonization in quantitative metallography, *Issues of Digital Image Processing*, R.M. Haralick and J.C. Simon, Eds. Groningen : The Netherlands: Stijthoff and Noordhoff, 1980..
37. J. Thirion, A. Gourdon, The 3D marching lines algorithm and its application to crest lines extraction, *Tech. Rep. RR-1672*, INRIA, Sophia Antipolis (1992).

38. Z. Chen, S. Malloi, Vessel diameter estimation in x-ray angiographic images using a watergauge algorithm, *Journal of Electronic Imaging* To appear.